Supporting Information

Preparation of M-$MnCo_2O_4$(M=Fe, Al, Bi, Cr) nanoenzymes with different doping ratios and detection of glutathione in serum

Meiqi Li[a], Qi Lian[a] , Xuefang Zheng[a,]*, Hongmei Yu[a] , Mengze Zhao[a] , Xiaojing Guo[a]

(a.College of Chemical Engineering, Hebei Normal University of Science and Technology, Qinhuangdao 066601, P. R. China)

*Corresponding author. E-mail: xuefang-zheng@163.com

Regents

Cobalt nitrate hexahydrate (Co $(NO_3)_3 \cdot 6H_2O$) purchased from Xi long Scientific Co.

3,3',5,5'-Tetramethylbenzidine (TMB) was purchased from Shanghai Jingchun Biochemical Technology Co.

Disodium hydrogen phosphate ($NaH_2PO_4 \cdot 2H_2O$) and citric acid ($C_2H_2O_7$) were purchased from Tianjin Chemical Reagent No.1 Factory.

Chromium nitrate hydrate ($Cr(NO_3)_3 \cdot 9H_2O$),manganese sulfate monohydrate ($MnSO_4 \cdot H_2O$), benzoquinone (BQ), glacial acetic acid (HAc), sodium acetate (NaAc), ferric nitrate hydrate ($Fe(NO_3)_3 \cdot 9H_2O$), isopropyl alcohol (IPA), bismuth nitrate pentahydrate ($Bi(NO_3)_3 \cdot 5H_2O$), and aluminum nitrate hydrate ($Al(NO_3)_3 \cdot 9H_2O$) were purchased from Tianjin Kai tong Chemical Reagent Co.

Glutathione (GSH) and oxalic acid ($H_2C_2O_4 \cdot 2H_2O$) were purchased from Tianjin Obo kai Chemical Co. Glucose, L-serine (Ser), histidine (His), glycine (Gly), alanine (Ala), L-threonine (Tyr), L-aspartic acid (Asp), and L-cysteine (Cys) were purchased from Aladdin reagent Co., Ltd. (China). All chemicals were of analytical grade at least.

Apparatus

For crystallographic analysis, X-ray diffractometer was utilized. X-ray diffractometer (XRD) patterns were recorded with Rigaku (SmartLab SE, Japan) at a scan rate of 8° per min with a scanning range of 10°-80° using Cu-Kα radiation (λ= 0.154 nm, 40 kV, 40 mA).

The physical form and architecture of the M-$MnCo_2O_4$(M=Fe, Al, Bi, Cr) were examined using a Hitachi SU-8010 scanning electron microscope (SEM) and a JEOL

JEM-2100F transmission electron microscope (TEM).

Fourier transform infrared (FT-IR) spectra were recorded on a FT-IR-Tensor 27 spectrometer (Bruker, Germany).

Raman spectrometer(Thermo fisher, DXR 532nm) was carried to characterize the as-synthesized M-$MnCo_2O_4$(M=Fe, Al, Bi, Cr) nanomaterials. A Spectra Physics solid-state laser operating at 532 nm was used for the excitation. The spectra were measured at 2 cm^{-1} spectral resolution and calibrated with a neon emission lamp.

Pore size characteristics and Specific surface area were quantified with a Micromeritics ASAP2460 surface area and a pore size analyzer. In addition, N_2 adsorption-desorption isotherms could be obtained by using this instrument(The sample was degassed at 300^oC for 3h).

Surface chemical com-position was analyzed via X-ray photoelectron spectroscopy (XPS) on a Thermo Fisher Scientific K-alpha spectrometer(The XPS spectrum was calibrated with foreign contaminated carbon C1s as the reference peak. The X-ray type was Mg-Kα. The data were processed and analyzed by the software Avantage).

Magnetic resonance properties were assessed using a MS-5000 Electron Paramagnetic Resonance (EPR) spectrometer from Bruker.

Zeta potential measurement: Electrochemical workstation. All the electrochemical experiments were performed on an electrochemical workstation (Autolab PGSTAT302N, Metrohm Co.) with a traditional three-electrode system with the GCE (3.0 mm in diameter) as the working electrode, Pt foil as the counter electrode, and a saturated calomel electrode (SCE) as the reference electrode.

Ultraviolet-visible light (UV-vis, UV-1800 PC) absorption spectra and absorbance measurements were recorded on a UV-1800 PC spectrophotometer (Perkin Elmer Instrument, USA).

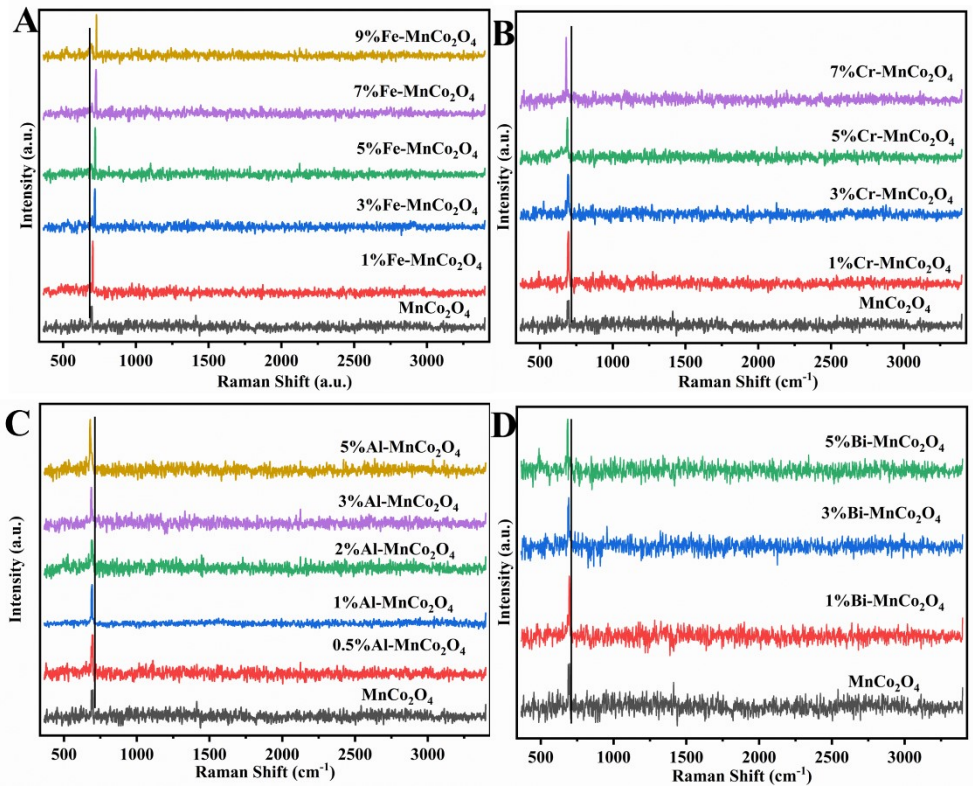

Figure S1. (A) Raman spectrum of Fe-$MnCo_2O_4$ with doping ratio of 0, 1%, 3%, 5%, 7%, 9%, (B) Raman spectrum of Cr-$MnCo_2O_4$ with doping ratio of 0,1%,3%,5%,7%, (C) Raman spectrum of Al-$MnCo_2O_4$ with doping ratio of 0, 0.5%, 1%, 2%, 3%, 5%, (D) Raman spectrum of Bi-$MnCo_2O_4$with doping ratio of 0, 1%, 3%, 5%.

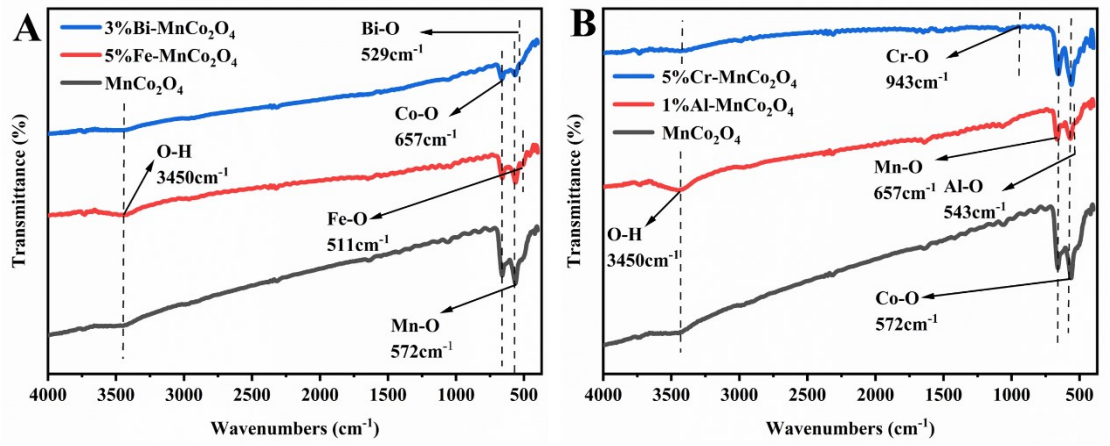

Figure S2. (A) FT-IR spectrum of 3%Bi-$MnCo_2O_4$, 5%Fe-$MnCo_2O_4$, $MnCo_2O_4$, (B) FT-IR spectrum of 5%Cr-$MnCo_2O_4$,1%Al-$MnCo_2O_4$, $MnCo_2O_4$.

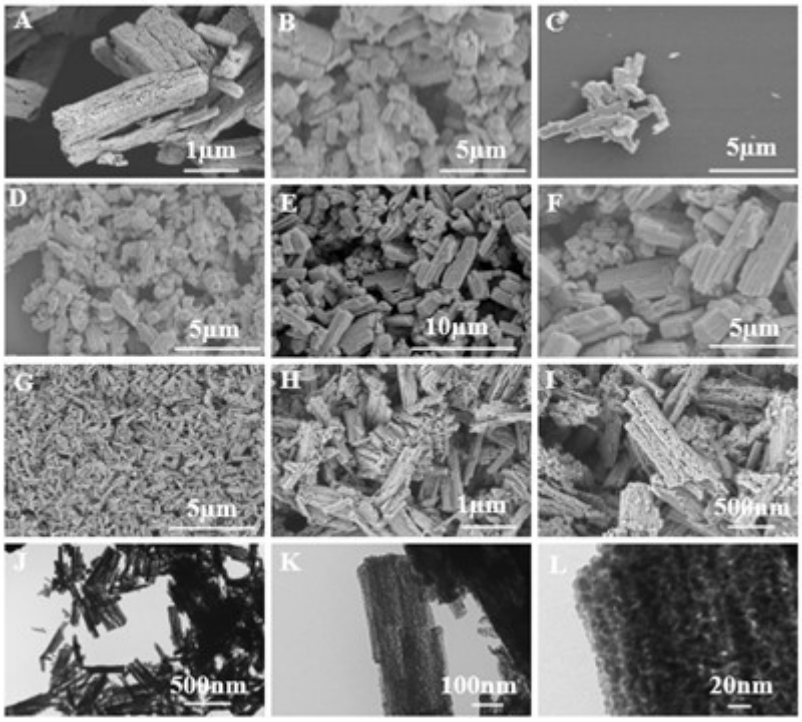

Figure S3. (A-D) SEM images of Cr-$MnCo_2O_4$ doped different Cr element with 0%, 1%, 3%, and 5%,respectively; (E-F) SEM images of 7% Cr-$MnCo_2O_4$ at different magnifications; (G-I) SEM images of 5% Cr-$MnCo_2O_4$ at different magnifications; (J-L) SEM images of TEM images of 5% Cr-$MnCo_2O_4$ at different magnifications;

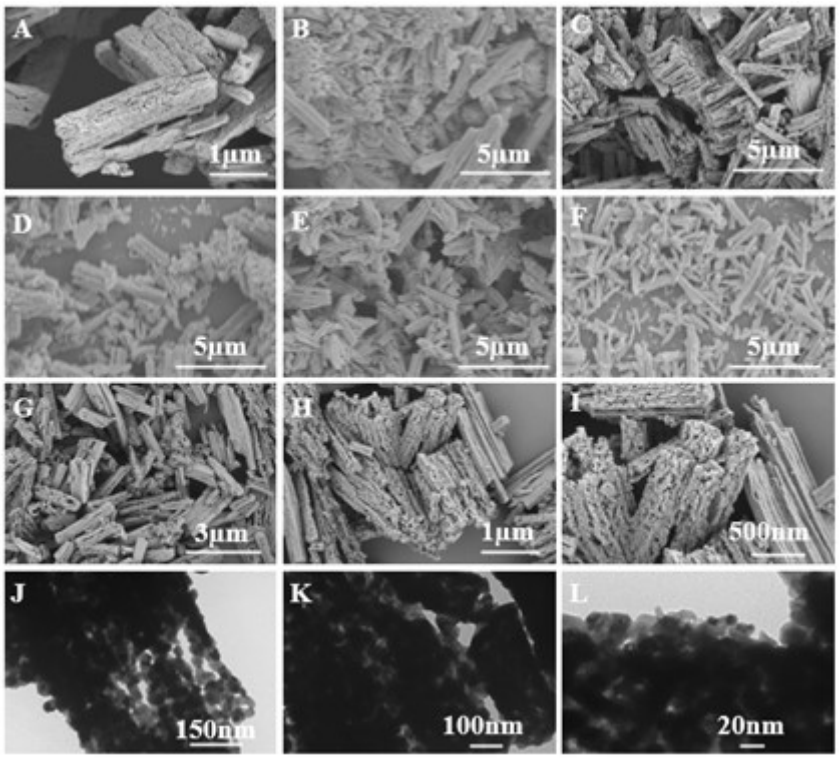

Figure S4. (A-F) SEM images of Al-$MnCo_2O_4$, doped Al element with different content of 0, 0.5%, 1%, 2%, 3%, and 5% respectively, (G-I) SEM images of 1% Al-$MnCo_2O_4$ at different magnifications, (J-L) TEM images of 1% Al-$MnCo_2O_4$ at different magnifications, respectively.

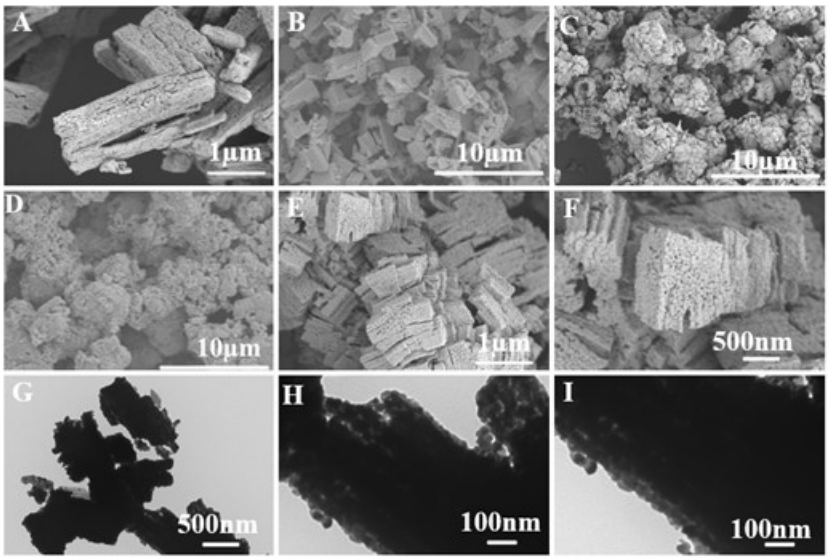

Figure S5. (A-D) SEM images of Bi-$MnCo_2O_4$ doped Bi element with different content of 0, 1%, 3%, and 5%, (E-F) SEM images of 3% Bi-$MnCo_2O_4$ at different magnifications, (G-I) TEM images of 3% Bi-$MnCo_2O_4$ at different magnifications, respectively.

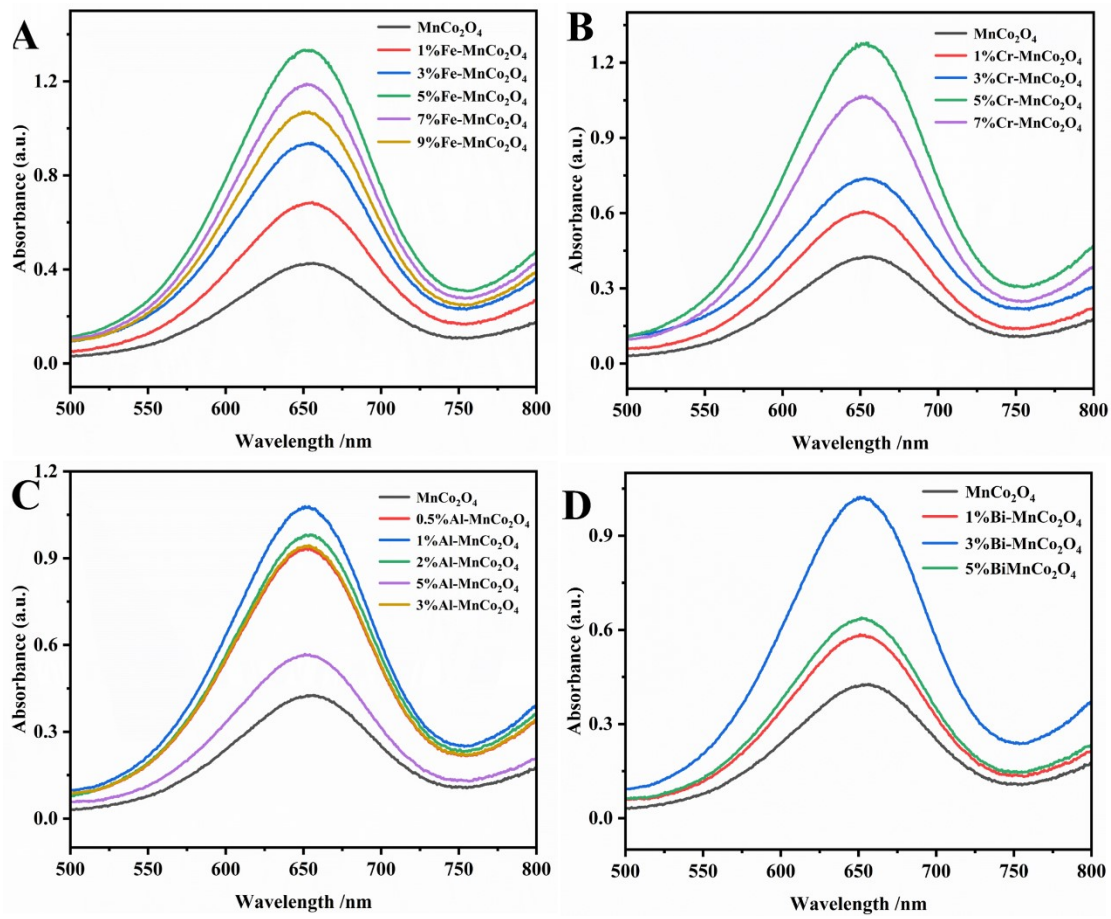

Figure S6. (A)UV-vis spectra of Fe-$MnCo_2O_4$ with doping of 0,1%,3%,5%,7%,9%, (B)UV-vis spectra of Cr-$MnCo_2O_4$ with doping of 0,1%,3%,5%,7%, (C)UV-vis spectra of Al-$MnCo_2O_4$ with doping of 0,0.5%,1%,2%,3%,5%, (D)UV-vis spectra of Bi-$MnCo_2O_4$ with doping of 0,1%,3%,5%.

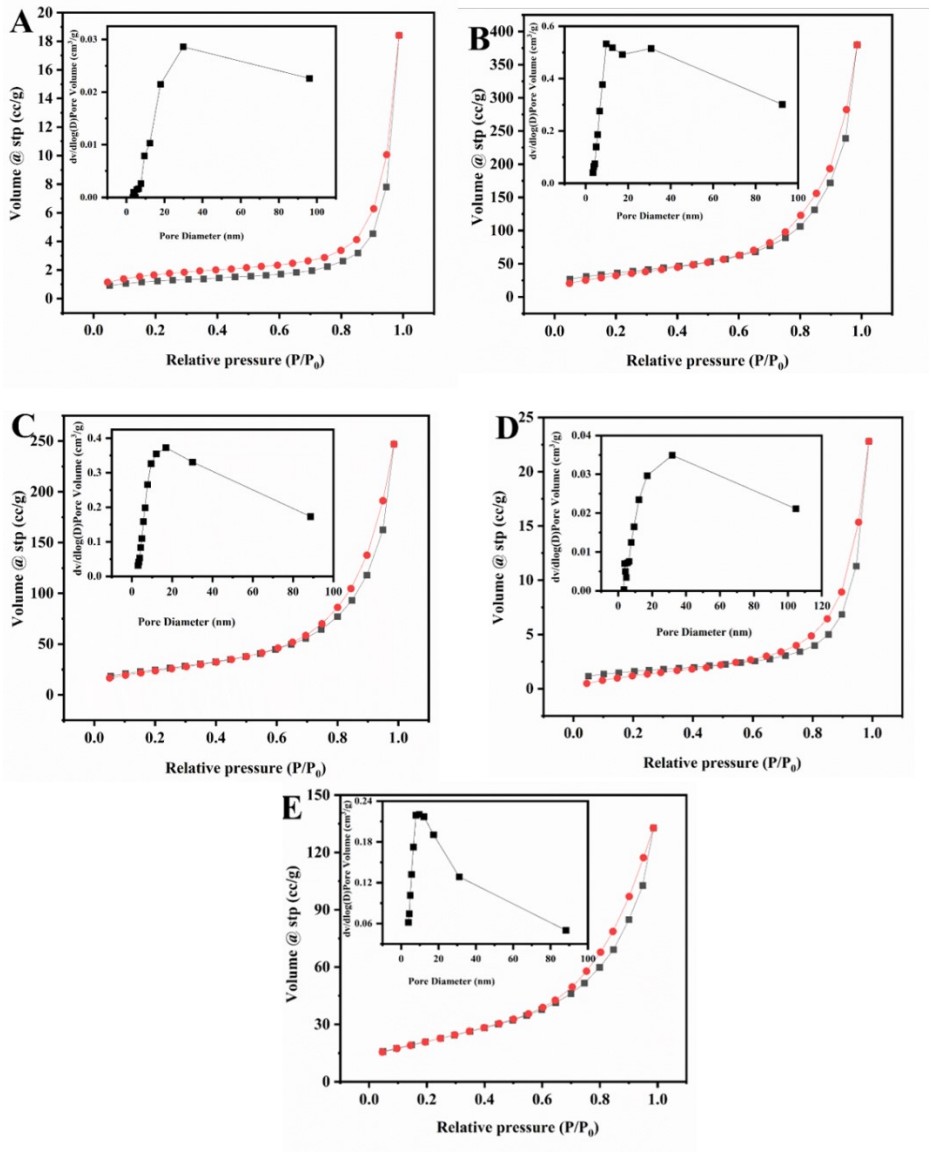

Figure S7. (A-E) N_2 adsorption-desorption of the $MnCo_2O_4$、M-$MnCo_2O_4$(M=Fe、Al、Bi、Cr) (Inset: corresponding pore size distribution)

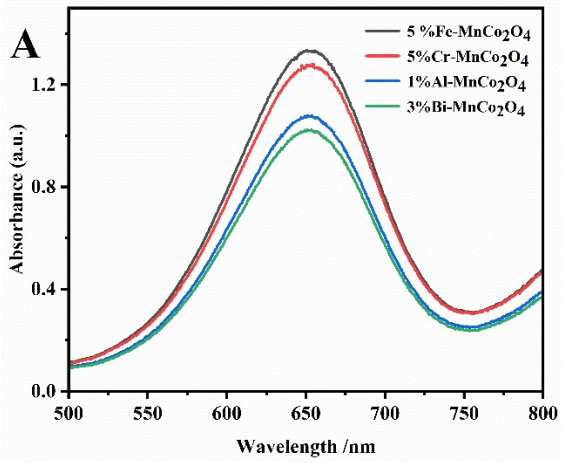

Figure S8. (A)UV-vis spectra of M-$MnCo_2O_4$(M=Fe、Cr、Al、Bi)

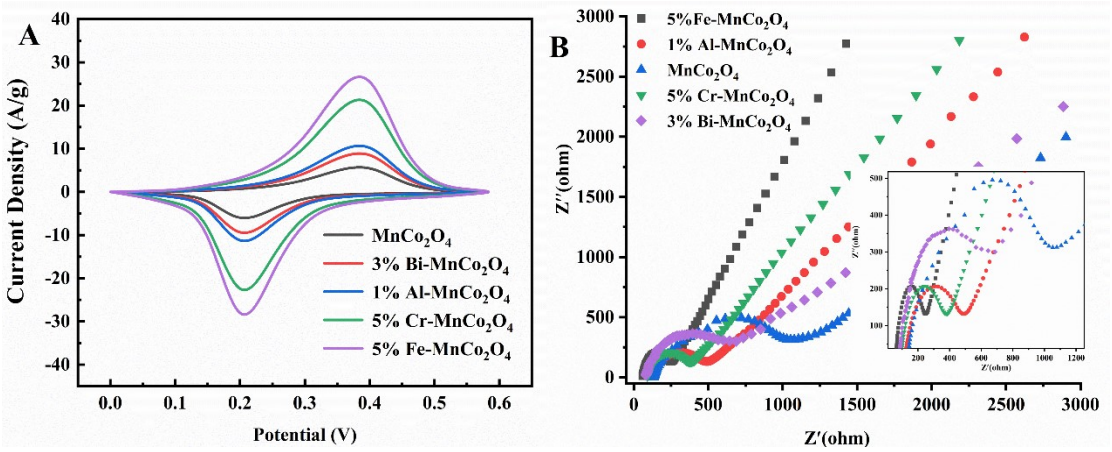

Figure S9. (A) Cyclic Voltammograms at scan rate 50mV s^{-1}, and (B) Nyquist impedance spectrum of 5%Fe-$MnCo_2O_4$、1%Al-$MnCo_2O_4$、$MnCo_2O_4$、5%Cr-$MnCo_2O_4$ and 3%Bi-$MnCo_2O_4$ materials.

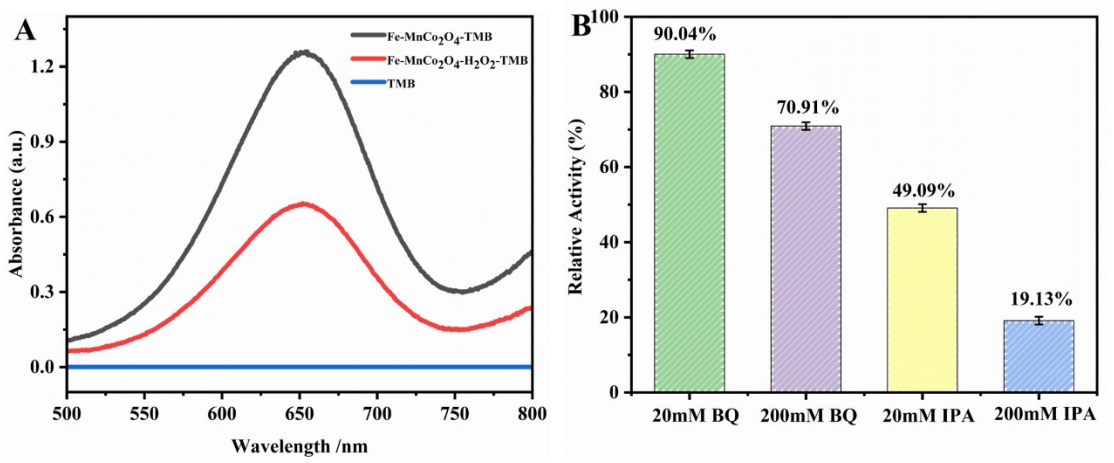

Figure S10. (A) the UV absorption curves of different systems (Fe-$MnCo_2O_4$-TMB, Fe-$MnCo_2O_4$-H_2O_2-TMB, TMB), Reaction conditions: t=10 min, pH=4, T=25°C, 15μg/ml 5% Fe-$MnCo_2O_4$, 120μM TMB, NaAc-HAc buffer (pH=4.0). (B) Effect of BQ (benzoquinone) and IPA (isopropyl alcohol) on the Fe-$MnCo_2O_4$-H_2O_2-TMB system.

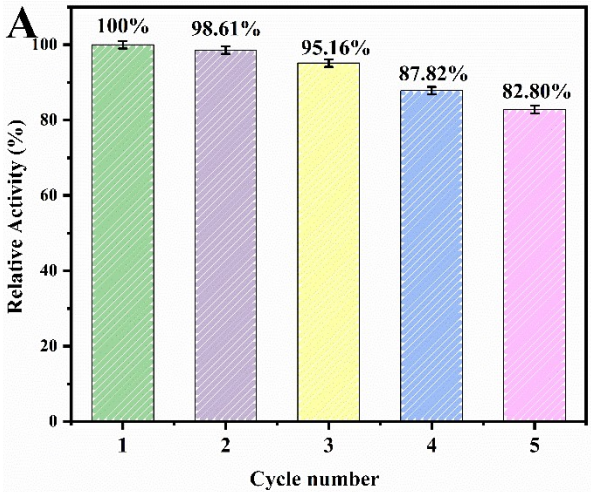

Figure S11. (A) Relative activity (%) of Fe-$MnCo_2O_4$ over 5 cycles under optimal reaction conditions.

Table S1. Comparison between Previously Reported Composites and Fe-$MnCo_2O_4$ Colorimetric Sensor for Detection of the Concentration of GSH

Materials	Method	LOD	Linear range	References
Fe-$MnCo_2O_4$	Colorimetric detection	0.1430μM	0-30μM	This work
Au	Colorimetric detection	0.5μM	0.5-1.25μM	33
Hg^{2+}-double-stranded DNA probe	Colorimetric detection	7.4nM	0.05-2.5μM	18
Sb-FeOCl	Colorimetric detection	0.495μM	1-36μM	34
MnO_2	Colorimetric detection	0.94μM	1-80μM	35
AuNP-PEDOT/GCE	Electrochemical detection	0.173μM	0.5-10μM	36
B-CDs	Colorimetric detection	0.62μM	0-20μM	37
Fe_3O_4-MnO_2	Colorimetric detection	0.2μM	0.2-25μM	38